ACS NANO

www.acsnano.org

ARTICLE

$Ti_3C_2T_x$ MXene-Reduced Graphene Oxide Composite Electrodes for Stretchable Supercapacitors

Yihao Zhou, Kathleen Maleski, Babak Anasori, James O. Thostenson, Yaokun Pang, Yaying Feng, Kexin Zeng, Charles B. Parker, Stefan Zauscher, Yury Gogotsi, Jeffrey T. Glass,* and Changyong Cao*

Cite This: *ACS Nano* 2020, 14, 3576–3586

Read Online

ACCESS | Metrics & More | Article Recommendations | Supporting Information

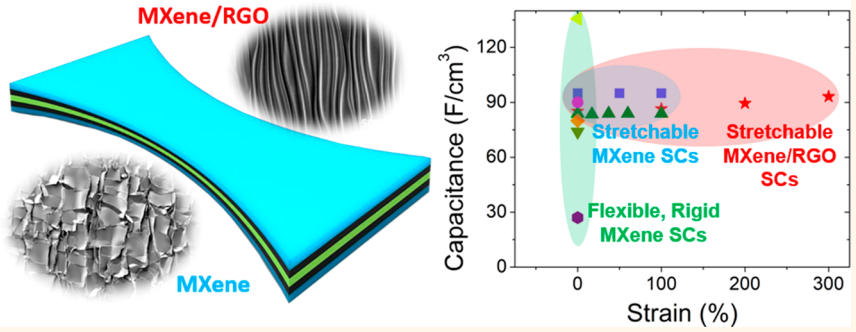

ABSTRACT: **The development of stretchable electronics requires the invention of compatible high-performance power sources, such as stretchable supercapacitors and batteries. In this work, two-dimensional (2D) titanium carbide ($Ti_3C_2T_x$) MXene is being explored for flexible and printed energy storage devices by fabrication of a robust, stretchable high-performance supercapacitor with reduced graphene oxide (RGO) to create a composite electrode. The $Ti_3C_2T_x$/RGO composite electrode combines the superior electrochemical and mechanical properties of $Ti_3C_2T_x$ and the mechanical robustness of RGO resulting from strong nanosheet interactions, larger nanoflake size, and mechanical flexibility. It is found that the $Ti_3C_2T_x$/RGO composite electrodes with 50 wt % RGO incorporated prove to mitigate cracks generated under large strains. The composite electrodes exhibit a large capacitance of 49 mF/cm^2 (~490 F/cm^3 and ~140 F/g) and good electrochemical and mechanical stability when subjected to cyclic uniaxial (300%) or biaxial (200% × 200%) strains. The as-assembled symmetric supercapacitor demonstrates a specific capacitance of 18.6 mF/cm^2 (~90 F/cm^3 and ~29 F/g) and a stretchability of up to 300%. The developed approach offers an alternative strategy to fabricate stretchable MXene-based energy storage devices and can be extended to other members of the large MXene family.**

KEYWORDS: *stretchable supercapacitors, MXene, reduced graphene oxide, composite electrodes, energy storage devices, stretchable electrodes*

Advances in stretchable electronics, such as stretchable displays,[1,2] artificial electronic skins,[3,4] wearable sensors,[5−7] and implantable devices,[8,9] have motivated the rapid development of compatible power sources (batteries and supercapacitors)[10,11] that are capable of stretching, deforming, or even conforming to integrate with a variety of stretchable devices and substrates. Compared with batteries that have the drawbacks of low cycle stability and power density, supercapacitors demonstrate exceptional power density, high cycle efficiency, and sufficient energy density for up to a million cycles. These features render stretchable supercapacitors a promising candidate for wearable and implantable energy storage devices.

Low-dimensional nanomaterials, such as carbon nanotubes (CNTs) and graphene, have been widely utilized for fabricating stretchable supercapacitors because of their excellent electrochemical performance, high surface area, and

Received: December 21, 2019
Accepted: February 12, 2020
Published: February 12, 2020

https://dx.doi.org/10.1021/acsnano.9b10066
ACS Nano 2020, 14, 3576–3586

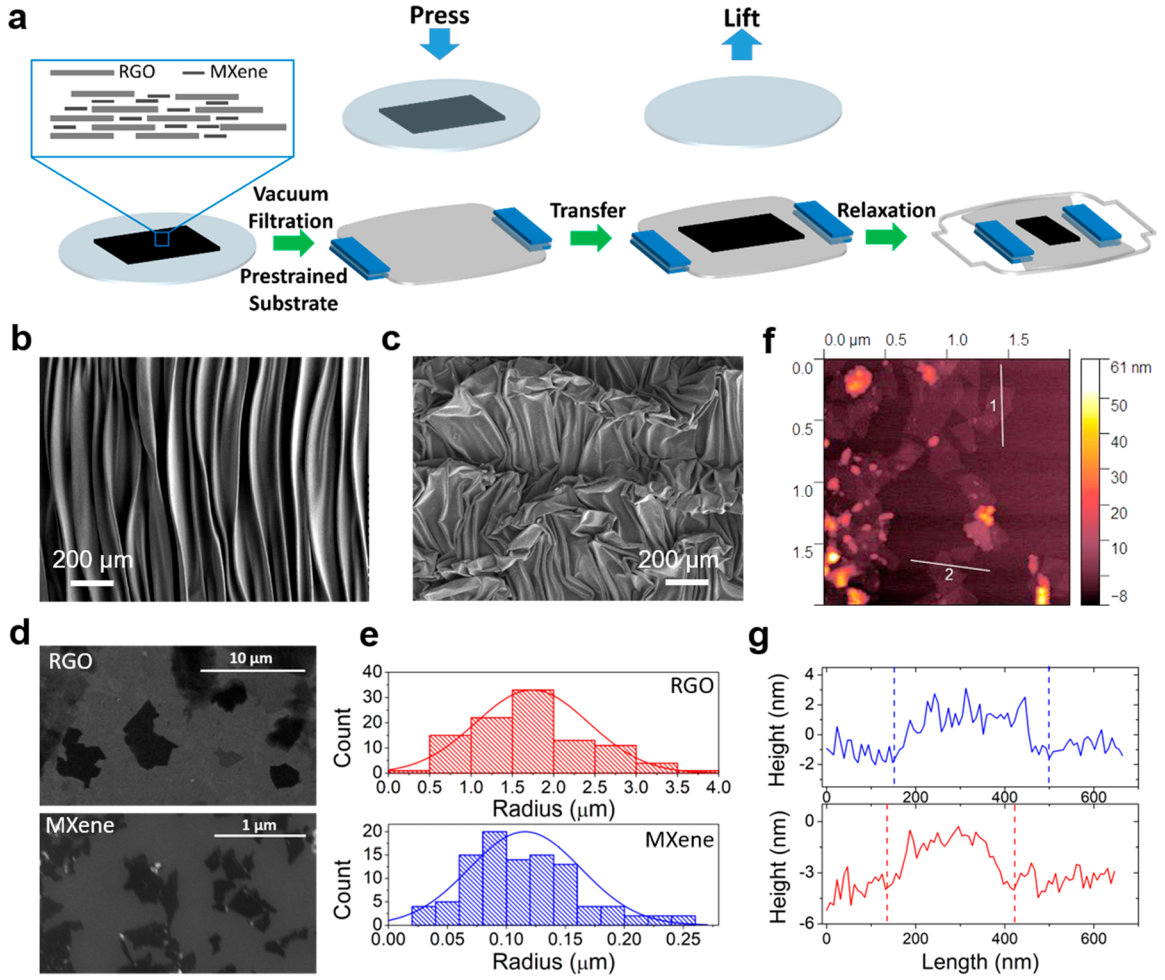

Figure 1. Fabrication and characterization of a stretchable $Ti_3C_2T_x$ MXene/RGO composite electrode. (a) Schematic illustration of the fabrication process of a stretchable $Ti_3C_2T_x$ MXene/RGO composite thin film electrode. (b) SEM image of the surface morphology of a $Ti_3C_2T_x$ MXene/RGO composite thin film (~1 μm) made by applying a uniaxial prestrain (300%). (c) SEM image of the surface morphology of a $Ti_3C_2T_x$ MXene/RGO composite thin film (~1 μm) made by applying a biaxial prestrain (200% × 200%). (d) SEM images of the RGO and $Ti_3C_2T_x$ MXene nanoflakes on Si wafer and (e) their size distributions obtained from SEM image analysis (with 100 flakes analyzed). (f) AFM image of the $Ti_3C_2T_x$ MXene nanoflakes. (g) Thickness profile of the $Ti_3C_2T_x$ MXene nanoflakes measured by AFM.

structural flexibility.[12] Another relatively new 2D material, $Ti_3C_2T_x$ (MXene),[13,14] has also been investigated for developing supercapacitors,[15] batteries,[16] sensors,[17] and electromagnetic interference shielding[18] due to its attractive properties: (1) metal-like electronic conductivity exceeding 10000 S/cm;[19] (2) hydrophilic surface groups enabling stable dispersion in water and various solvents;[20] and (3) high volumetric capacitance up to 1500 F/cm^3.[21] Although MXenes have been successfully applied to develop both rigid and flexible electrochemical supercapacitors,[22,23] microsupercapacitors,[24,25] and metal-ion batteries,[26−28] MXene-based stretchable electronics and energy-storage devices are rarely reported due to the challenges and constraints originating from the high modulus of elasticity (3−75 GPa in a dry state)[29] and fragility of MXene films made of micrometer-sized flakes after drying.[30] For example, An *et al.* presented a strain sensor based on MXene/poly(diallyl dimethylammonium chloride), capable of stretching up to 40% strain.[31] However, at the stretched state, the resistance of the device increased by an order of magnitude, which does not meet the requirements for stretchable energy storage applications where devices should maintain their performance under even larger tensile strains. Recently, Chang *et al.* developed a stretchable supercapacitor with MXene/carbon black/sodium alginate electrodes and obtained good performance when it was subjected to tensile strains in the range of 80−100%, but a complicated and time-consuming manufacturing was required.[32] Also, the organic molecules incorporated into the stretchable MXene supercapacitors may block the accessible surface area of the MXene sheet, decreasing specific capacitance. Therefore, it is desirable to develop a robust supercapacitor by using nanomaterials which have chemical stability, superior electrochemical performance, high stretchability, and allow for a simple fabrication process.

In this work, we have developed a procedure to fabricate stretchable supercapacitor electrodes using $Ti_3C_2T_x$ MXene-based composites by adding compliant reduced graphene oxide (RGO) with stronger intersheet interaction and larger nanoflake size. The $Ti_3C_2T_x$/RGO composite electrodes keep structural integrity and electrical conductivity under large cyclic strains (*i.e.*, uniaxial 300% and biaxial 200% × 200% strains). In contrast, the pure $Ti_3C_2T_x$ electrodes break into small pieces and display many cracks, leading to dramatically decreased electrochemical performance. The as-

https://dx.doi.org/10.1021/acsnano.9b10066
ACS Nano 2020, 14, 3576−3586

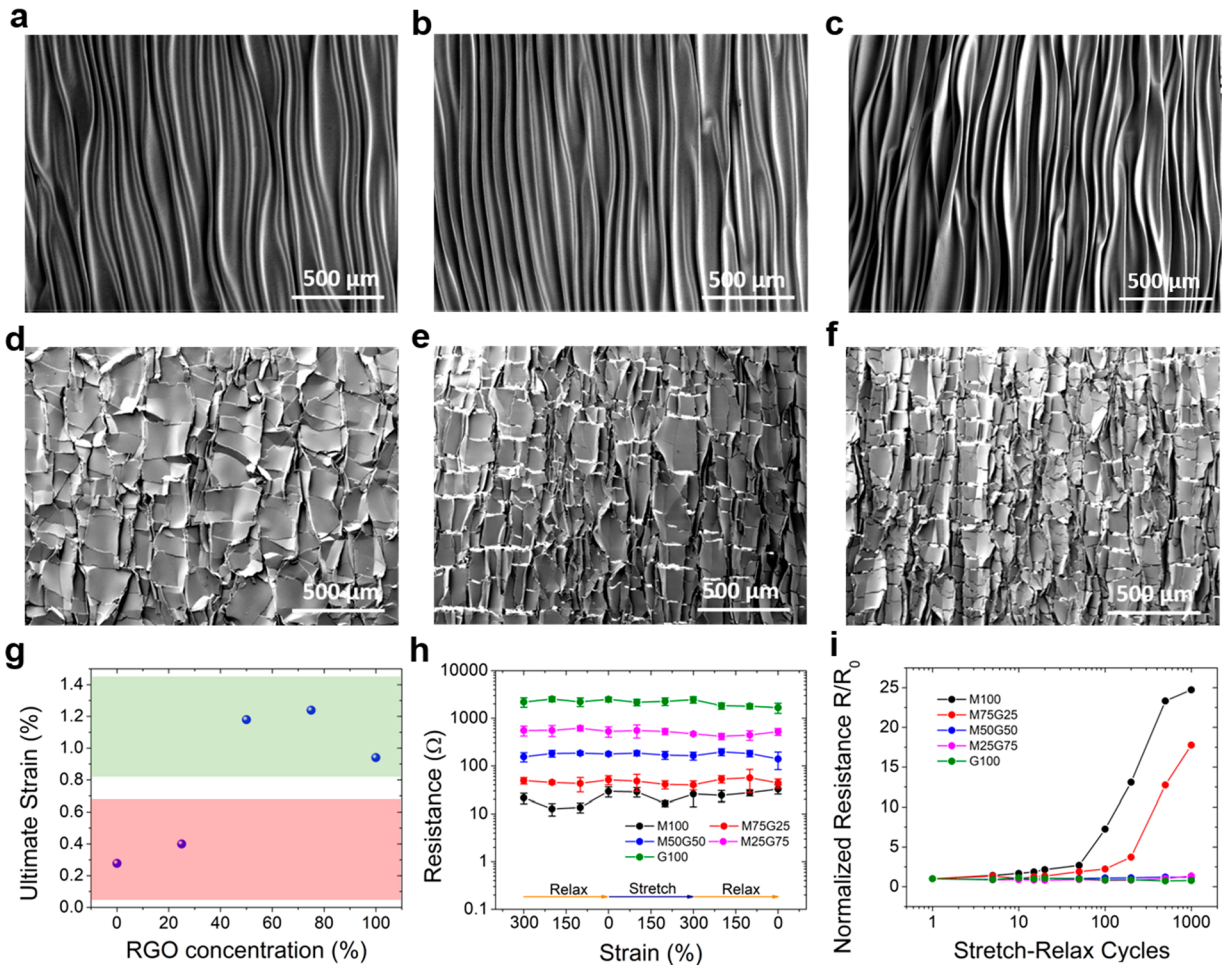

Figure 2. Mechanical and electrical characterization of the $Ti_3C_2T_x$ MXene/RGO composite films with different percentages of RGO. (a–c) SEM images of $Ti_3C_2T_x$ MXene/RGO thin films (~1 μm) at their relaxed states, made by applying a prestrain of 100%, 200%, and 300%, respectively. The composite film maintains the wrinkles/ridges pattern well. (d–f) SEM images of pure $Ti_3C_2T_x$ MXene thin films (~0.6 μm) at their relaxed states, made by applying a prestrain of 100%, 200% and 300%, respectively. Many cracks generate after releasing the substrate prestrain. (g) Ultimate strain of the $Ti_3C_2T_x$ MXene/RGO composite films as a function of the RGO concentration. (h) Variations of the electrical resistances of the $Ti_3C_2T_x$ MXene/RGO composite films with different percentages of RGO as a function of applied stretching strains from 0 to 300%. (i) The normalized electrical resistances of the $Ti_3C_2T_x$ MXene/RGO composite films with different percentage of RGO subjected to cyclic stretching strain of 250% for up to 1000 cycles.

prepared $Ti_3C_2T_x$/RGO composite electrodes retain their conductivity after uniaxial stretching up to 250% strain for over 1000 stretching–relaxation cycles. $Ti_3C_2T_x$/RGO composite electrodes demonstrate the highest stretchability and consistent electrochemical performance under extremely large strains (uniaxially 300% and biaxially 200% × 200%), exhibiting a specific areal capacitance of 49 mF/cm^2 (volumetric capacitance of ~490 F/cm^3 and gravimetric capacitance of ~140 F/g). Finally, an all-solid-state stretchable $Ti_3C_2T_x$/RGO supercapacitor has been fabricated, and demonstrates an excellent electrochemical stability and a specific capacitance of ~18.6 mF/cm^2 (volumetric capacitance of ~90 F/cm^3 and gravimetric capacitance of ~29 F/g). This research offers an alternative strategy to fabricate high-performance stretchable supercapacitors with MXene, and it can also be extended to utilize other materials in the MXene family for flexible electronics and energy devices.

RESULTS AND DISCUSSION

Fabrication and Characterization of Thin Film Electrodes. Figure 1a shows the fabrication process of a stretchable MXene/RGO composite film electrode. In brief, a MXene/RGO composite film is fabricated by vacuum-assisted filtration of a solution of MXene and RGO dispersed in deionized water (Millipore) with a weight ratio of 1:1. Then an acrylic elastomer substrate (VHB 4910, 3 M, Inc., US) is stretched to a specific strain, *i.e.*, 300% uniaxially, and fixed for the dry transfer of the film. The top surface of the as-prepared MXene/RGO composite film that was resting on the nitrocellulose filter membrane (0.05 μm pore size, Merck Millipore Ltd., Ireland) is pressed onto the prestrained elastomer substrate by hand, and then the filter membrane is slowly peeled off to transfer the MXene/RGO composite onto the stretched elastomer substrate. Because the adhesion force between the polymer substrate and the MXene/RGO composite paper is much larger than the force between the MXene/RGO composite film and the filter membrane, the MXene/RGO composite film can be easily transferred to the elastomer substrate. After the dry-transfer step, the substrate is slowly relaxed along the prestrained direction, allowing the substrate to restore its original length and form a wrinkled/ridged pattern (Figure 1b). Different magnifications of SEM

https://dx.doi.org/10.1021/acsnano.9b10066
ACS Nano 2020, 14, 3576–3586

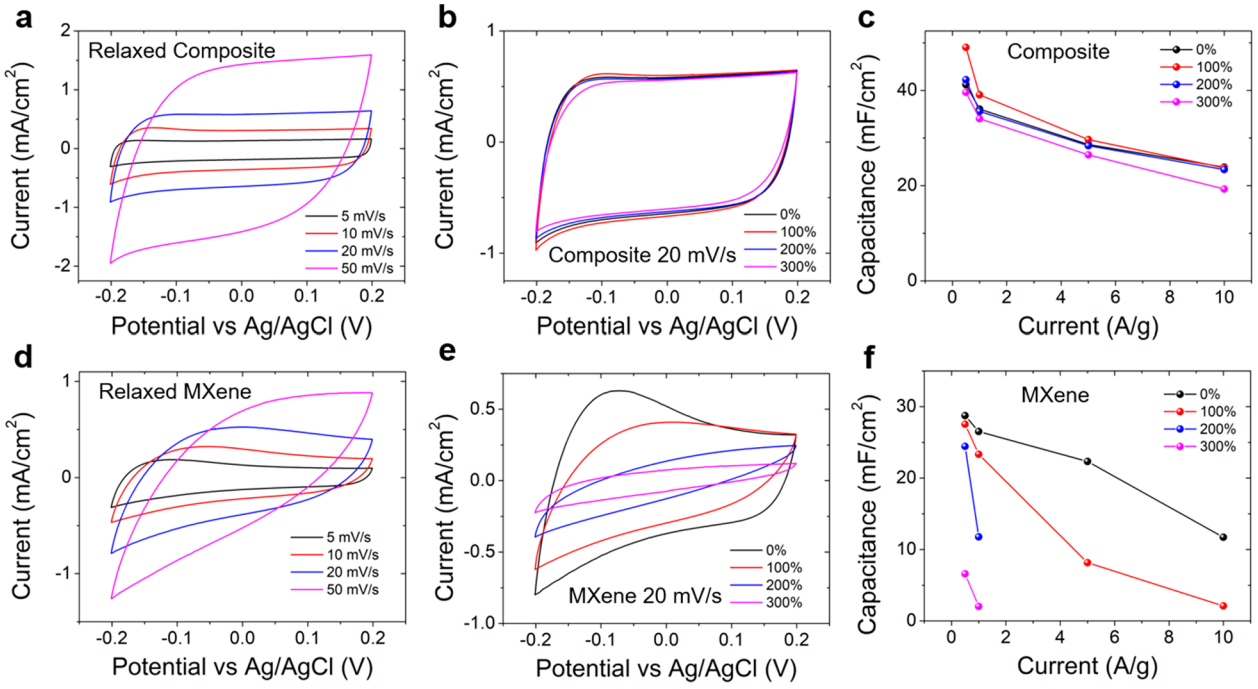

Figure 3. Electrochemical performance of a stretchable $Ti_3C_2T_x$/RGO electrode and a pure $Ti_3C_2T_x$ MXene electrode. (a) Cyclic voltammogram (CV) curves of the$Ti_3C_2T_x$/RGO electrode measured at different scan rates in the relaxed state. (b) CV curves of a $Ti_3C_2T_x$ MXene/RGO electrode measured at 20 mV/s scan rate under different tensile strains (0 to 300%). (c) Specific capacitances calculated by galvanostatic charge−discharge (GCD) measurements of a $Ti_3C_2T_x$ MXene/RGO electrode at different charge/discharge current densities under strains from 0 to 300%. (d) CV curves of a $Ti_3C_2T_x$ MXene stretchable supercapacitor electrode measured at scan rates from 5 to 50 mV/s in the relaxed state. (e) CV curves of the MXene electrode measured at the scan rate of 20 mV/s under tensile strains from 0 to 300%. (f) Specific capacitances calculated from GCD measurements of the $Ti_3C_2T_x$ MXene electrode at different strain states and different charge/discharge current densities. When the tensile strain is larger than 200%, the overall resistance of the $Ti_3C_2T_x$ MXene film becomes very large due to the cracking of the electrode film, leading to dramatic ohmic drop and zero capacitance.

images for the MXene/RGO composite thin film in Figure S1 show that the wavelength of wrinkles/ridges is approximately 50 μm. Following the same procedures above, biaxially stretchable MXene/RGO composite electrodes were also fabricated (*e.g.*, 200% × 200% prestrain in two orthogonal directions) (Figure 1c and Figure S2).

It can be seen from the SEM images in Figure 2a−c that the wrinkled/ridged composite films maintain their structural integrity without any visible cracks formed by applying different uniaxial prestrains of 100%, 200%, and 300%, respectively. On the contrary, cracking and fragmentation of the pure MXene electrode films fabricated with the same procedures from all three different prestrains was observed, as shown in Figure 2d−f. The cracks generated in the relaxation process are attributed to the high mechanical modulus and small flake size in MXene films.[29,33] Compared with MXene, the RGO films possess a lower Young's modulus (<1.5 GPa), stronger intersheet interaction, and higher elongation-at-break,[34] making it more compliant to the extreme mechanical deformations in the relaxation process. Additionally, the size of RGO nanoflakes in the composite is measured as 1.74 ± 0.68 μm, whereas the flake size of MXene is 0.116 ± 0.047 μm (Figure 1d). The small size of the MXene flakes is important to facilitate ionic transport and achieve good electrochemical properties. The larger RGO flake size leads to stronger intersheet interactions by increasing the face-to-face interaction area and reducing the edge-to-edge interactions.[35] It has been reported that the energy of the face-to-face interaction increases with the flake size and is much larger than the edge-to-edge interaction.[36] Additionally, the larger flake size can have a positive effect on the alignment of the nanoflakes in the vacuum filtration process through the "excluded volume" interactions. As a result, the MXene/RGO composite film exhibits higher flexibility and larger toughness[37] and stays intact under large mechanical deformations or strains. The average thickness of a MXene nanoflake measured by atomic force microscopy (AFM) is ∼2.6 nm and corresponds to single- or double-layer flakes (Figure 1g), consistent with a previous literature report,[30] while the thickness of a single RGO layer is ∼1.2 nm (Figure S4). RGO nanoflakes with smaller thickness render lower bending stiffness, which is also beneficial for the flexibility of the film in the stretching-releasing deformations.

The surface energies of single-layer RGO and MXene nanoflakes on a SiO_2 substrate are then measured by lateral force microscopy (LFM) using a Si cantilever tip (Figure S5a,b and d,e). The cross-sectional profiles of the friction force of the MXene and RGO flakes are shown in Figure S5c. These profiles show that the friction force of the Si tip is lower for MXene surfaces and higher for RGO surfaces compared to the friction on the SiO_2 substrate. This suggests that MXene flakes have a lower surface energy than RGO flakes (Figure S5f). We attribute the larger surface energy of the RGO flakes to the presence of carboxyl and hydroxyl groups on their surfaces.[38] The larger surface energy of RGO flakes may lead to stronger intersheet interactions between RGO flakes, and RGO and MXene flakes, which also benefits the formation of more robust composite films compared to those obtained with MXene flakes alone.

https://dx.doi.org/10.1021/acsnano.9b10066
ACS Nano 2020, 14, 3576−3586

MXene/RGO composite films with RGO weight percentages ranging from 0% to 100% were fabricated and tested to further study the effect of the RGO on the electrical and mechanical properties. Figure 2g presents the variation of the ultimate strain (elongation to failure in the stress−strain curves in Figure S6) of MXene/RGO composite films as a function of the RGO percentage. It is observed that the ultimate strain increases with increasing RGO percentage. When the weight percentage of RGO is greater than 50%, the ultimate strain of the MXene/RGO composite film reaches ∼1% and remains almost constant. As shown in Figure 2a−c, the stretchability of MXene/RGO thin films with RGO percentage >50% enables the electrode films to remain intact during the stretching-relaxation process.

The electrical stability as a function of cycling was tested by measuring the resistance while applying a uniaxial strain of up to 250% for 1000 stretching-relaxation cycles. The measurements show that MXene/RGO composite films with >50% percentage of RGO maintain a stable resistance after 1000 mechanical cycles (Figure S3), while the resistance of the MXene/RGO composite thin films with RGO percentage of 0% or 25% gradually increases with the mechanical cycles, indicating the separation or disconnection of the cracked MXene/RGO film pieces. It is noted that although many cracks are formed in the pure MXene film during the initial relaxation process (Figure 2d−f), the overall resistance of the MXene film remains small during the first few stretching-relaxation cycles (Figure 2h). The low resistance of the MXene film indicates that the cracked MXene flakes are still electrically connected until approximately 50 cycles. After 50 stretching-relaxation cycles, the resistance of the pure MXene film increases significantly and reaches ∼800 Ω after 1000 mechanical cycles (∼25 times of its original value, as shown in Figure 2i). Compared to the pure MXene film, the resistance of the MXene/RGO composite (50 wt %) stays constant and maintains ∼150 Ω after 1000 mechanical cycles. Therefore, the MXene/RGO composite film is more suitable than the pure MXene film for most stretchable applications, and the composite is more suitable than pure RGO for electronic applications.

Electrochemical Performance. The resistance of the MXene/RGO composite film increases with the percentage of RGO (Figure 2h) indicating a trade-off between the stability and the electrical conductivity determined by the composition. For applications requiring thousands of loading cycles, the MXene/RGO composite film with RGO of 50 wt % possesses the best combination of electrical conductivity and mechanical robustness. Thus, this MXene/RGO composition was chosen for further testing as a supercapacitor electrode and compared with pure MXene films. Figure 3a−c shows the electrochemical performance of a stretchable MXene/RGO composite electrode, where the cyclic voltammetry (CV) curves of the stretchable MXene/RGO composite electrode at 0% strain are rectangular from 5 to 50 mV/s, showing a double-layer capacitive behavior in the selected narrow voltage window. CV curves of the stretchable MXene/RGO composite electrode under different strain states are almost identical (Figure 3b and Figure S7) due to the electrochemical properties of MXene and the structural integrity of composite film maintained under large deformations. Figure 3c presents the specific capacitance of the stretchable MXene/RGO composite electrode from the galvanostatic charge/discharge (GCD) curves at different strain states. At a small current density of 0.5 A/g, the measured specific capacitance can reach ∼40 mF/cm^2. However, when the current density increases to 10 A/g, the measured specific capacitance drops to ∼20 mF/cm^2 corresponding to about 50% capacitance retention. The electrochemical stability of the MXene/RGO composite electrodes under different strains indicates that the pore structure and accessible active materials may remain the same under large deformations. The consistent electrochemical performance of MXene/RGO composite electrodes at different strain states demonstrates that the MXene/RGO composite film is a promising candidate for stretchable supercapacitor electrodes.

In contrast to the MXene/RGO composite electrodes, pure MXene supercapacitor electrodes show dramatically decreased electrochemical performance under large deformations. Figure 3d presents the CV curves of a pure MXene electrode at 0% strain state and shows that the CV curves become highly distorted (resistive) when the scan rate increases to 50 mV/s, confirming the large resistance caused by MXene film cracking. When a uniaxial strain is applied to the electrode, the distance between cracked MXene flake pieces increases, resulting in further reduction of the film conductivity. As a consequence, the electrochemical performance of the pure MXene electrode deteriorates under large mechanical strains from 100% to 300% (Figure S7). Figure 3e compares the CV of the MXene electrode under different strains at 20 mV/s. It is clear that the capacitive current of the pure MXene film decreases significantly as the applied strain increases. The specific capacitance (Figure 3f) reveals that the electrochemical performance of the pure MXene electrode is significantly affected by the applied strain.[15] The specific capacitance of the MXene electrode at 1 A/g drops over 50% when a 200% strain is applied, indicating the loss of active material resulting from the electrical disconnection of cracked MXene flakes during the deformation. Moreover, the device fails at current densities larger than 1 A/g under the strain of 200% or 300% because high internal resistance leads to an ohmic drop exceeding the measurable potential range.

Additional details about the properties of the pure MXene and MXene/RGO composite film electrodes can be obtained from electrochemical impedance spectroscopy (EIS) measurements (Figure S8). Figure S8a,c and Figure S8b,d present the Nyquist plots of pure MXene film electrodes and MXene/RGO composite film electrodes at low frequencies and middle-to-high frequencies, respectively. The small resistance at 200 kHz (∼0.6 Ω) indicates the high conductivity of the electrolyte. For the pure MXene film electrode, the resistance (semicircle) at middle-to-high frequency range increases from ∼25 to ∼200 Ω with applied strains, which is attributed to the increased film resistance under larger deformations. The slope of EIS curves gradually decreases at low frequencies, indicating the transition from a capacitive to a resistive response. The increase of the corresponding real and imaginary impedance implies less ionic access to the electrode surface and lower conductivity of the film, consistent with the results of CV and GCD tests. For the MXene/RGO composite electrode, the semicircle in the Nyquist plot maintains nearly the same values (∼8−14 Ω) at different strains, agreeing well with the overlapped CV of the MXene/RGO composite electrode in Figure 3e. Additionally, similar slopes (near vertical) at the low frequency range represent identical capacitive behavior of the MXene/RGO composite electrode under different strains, also in good agreement with the CV and GCD measurements.

https://dx.doi.org/10.1021/acsnano.9b10066
ACS Nano 2020, 14, 3576−3586

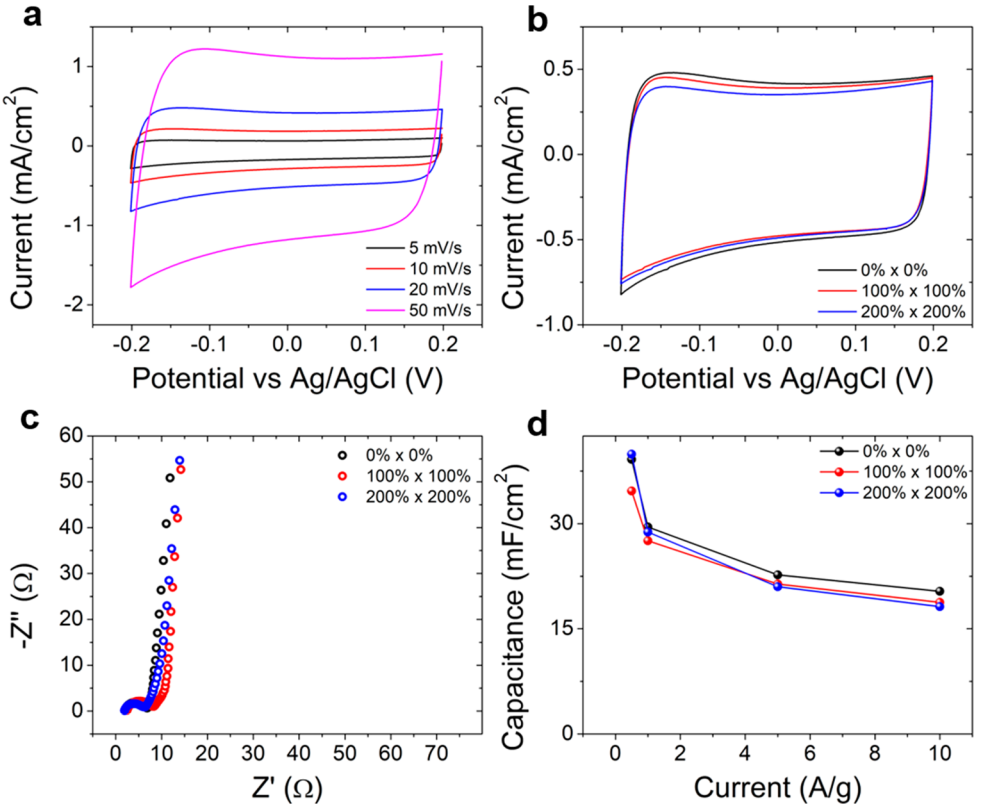

Figure 4. Electrochemical performance of a biaxially stretchable $Ti_3C_2T_x$ MXene/RGO composite supercapacitor electrode. (a) CV curves of the $Ti_3C_2T_x$ MXene/RGO electrode measured at different scan rates under relaxed state. (b) CV curves of the $Ti_3C_2T_x$ MXene/RGO electrode measured at 20 mV/s scan rate under different biaxial stretching strains. (c) Nyquist plot of the $Ti_3C_2T_x$ MXene/RGO electrode under different biaxial strains. (d) Specific capacitances calculated by GCD measurements of the $Ti_3C_2T_x$ MXene/RGO electrode at different charge/discharge current densities under different stretching strains.

Figure 4 shows the electrochemical performance of a biaxially stretchable MXene/RGO electrode (200% × 200%). Compared with the uniaxially stretchable MXene/RGO electrode, the local deformation of the biaxially stretchable MXene/RGO is larger (Figure 1c). However, due to the incorporation of RGO into MXene, the composite electrode is not broken/cracked during the stretching-relaxation deformation process. The CV curves of the biaxially stretchable MXene/RGO electrode retain the square-shape at different scan rates, indicating its excellent electrochemical performance (Figure 4a), and consistent with CV measured at 20 mV/s under various area strains ranging from 0% to 800% (Figure 4b). The EIS curves of the biaxially stretchable MXene/RGO composite electrode exhibit similar semicircles (~4−6 Ω for all strain states) and slopes at both high and low frequency ranges, indicating a robust electrochemical performance of the composite electrode under extreme large strains (Figure 4c). Figure 4d shows the specific capacitance of the MXene/RGO composite electrode under different biaxial strains (0% × 0%, 100% × 100%, 200% × 200%). It can be seen that the applied strain has little influence on the specific capacitance of the MXene/RGO composite electrode. However, the capacitance decreases from ~36 mF/cm^2 at 0.5 A/g to ~18 mF/cm^2 at 10 A/g with the increased current density for different strain states, which is consistent with the results of uniaxially stretchable MXene/RGO composite electrodes.

All Solid-State Supercapacitors. To demonstrate the performance of supercapacitor devices, all-solid-state stretchable supercapacitors with the stretchable MXene/RGO composite electrodes and PVA-H_2SO_4 gel electrolyte were fabricated (Figure 5a). The measured CV curves of a symmetric supercapacitor show a somewhat distorted rectangular shape at scan rates from 5 to 20 mV/s at the strain of 0%, *i.e.*, in the relaxed state (Figure 5b), indicating a capacitive behavior of the electrodes. However, the shape of the CV curve is resistive at 50 mV/s, revealing an increased influence of the internal resistance in the electrode at high current density. This is further confirmed by the large intercept (140 Ω) on the Z' axis in the Nyquist plot (Figure 5d). The large film resistance is attributed to the poor conductivity of RGO. Nonetheless, the supercapacitor shows stable electrochemical performance when it is subjected to different applied strains (Figure 5c). Similar slopes of the impedance spectra under different strains at low frequency further confirm that the MXene/RGO stretchable supercapacitor maintains its electrochemical performance under large mechanical deformations. Figure 5e shows the measured results of the MXene/RGO supercapacitor by GCD tests under different strains. The triangular shape of the charge−discharge curves verifies that the main charge storage mechanism in the measured potential range is the electrochemical double layer (EDL). Similar charge/discharge times for GCD cycles indicate similar capacitances for the MXene/RGO supercapacitor at different strain states, which is consistent with the CV and EIS measurements. The specific capacitance of the MXene/RGO supercapacitor is calculated as 18.6 mF/cm^2 at the scan rate of 0.1 A/g, based on the GCD tests (Figure 5f), which is consistent with the measured value (~40 mF/cm^2) of a single

https://dx.doi.org/10.1021/acsnano.9b10066
ACS Nano 2020, 14, 3576−3586

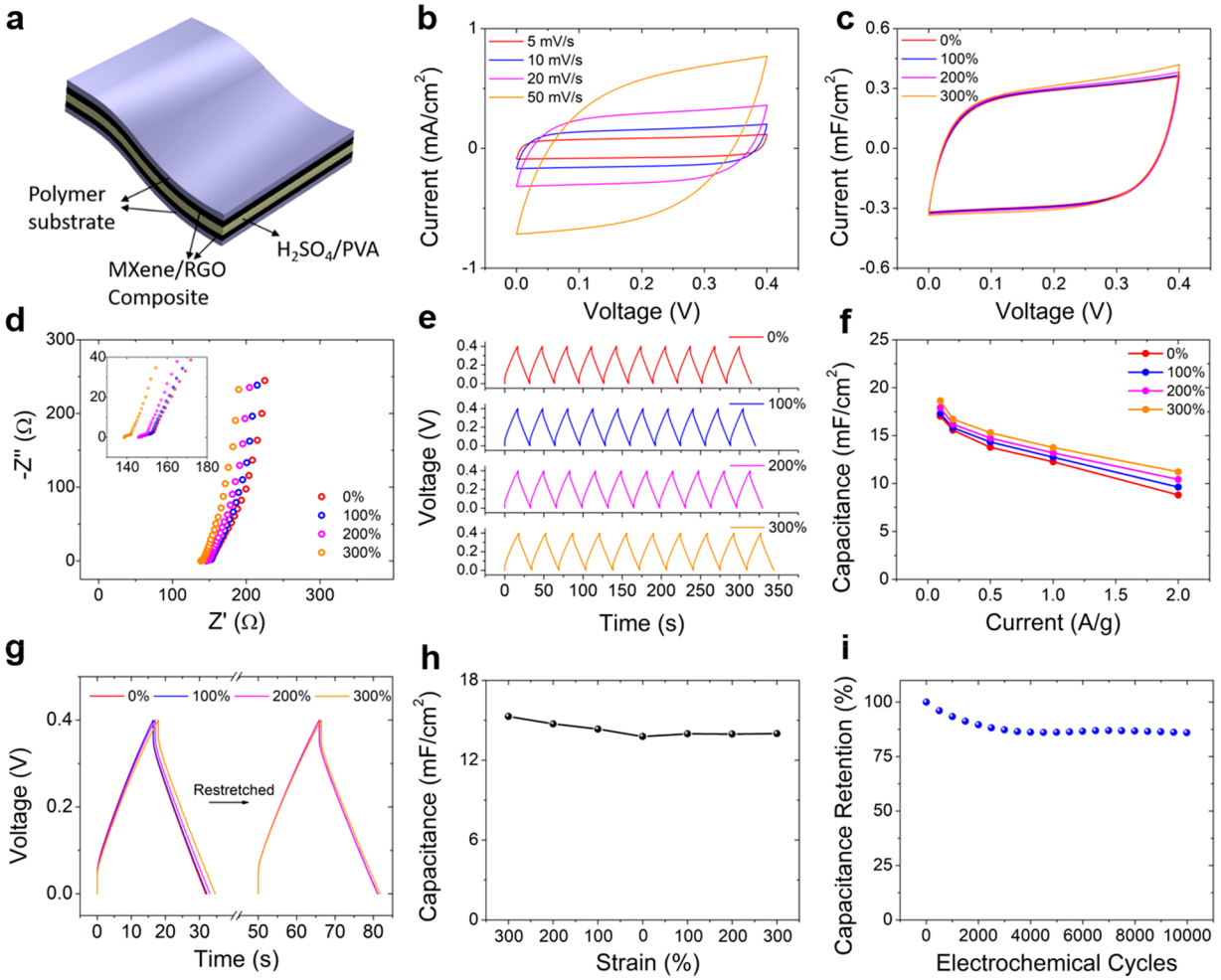

Figure 5. Electrochemical performance of a stretchable supercapacitor with stretchable $Ti_3C_2T_x$ MXene/RGO composite electrodes and sulfuric acid poly(vinyl alcohol) (H_2SO_4/PVA) gel electrolyte. (a) Scheme of the stretchable $Ti_3C_2T_x$ MXene/RGO composite supercapacitor. (b) CV curves of the stretchable SC measured at different scan rates in the relaxed state. (c) CV curves of the stretchable SC at 20 mV/s scan rate under different stretching strains. (d) EIS of the stretchable SC at different strain states. (e) GCD curves of the stretchable SC subjected to different strains and measured at 0.5 A/g. (f) Specific capacitance of the stretchable SC measured at different strains and different charge/discharge current densities. (g) Constant current charge/discharge (0.5 A/g) curves of the stretchable SC in a mechanical relax−stretch cycle. (h) Specific capacitance of the stretchable SC in a mechanical relax−stretch cycle at the charge/discharge current density of 0.5 A/g. (i) Electrochemical stability of the stretchable SC for 10000 charge/discharge cycles.

electrode considering the halved capacitance in the device. The specific capacitance of the supercapacitor is maintained over all measured current densities at different strain states due to the structural integrity of the MXene/RGO composite electrode.

As shown in Figure 5g,h, the capacitance of the stretchable supercapacitors exhibits little variation (8%) during multiple stretching−relaxation cycles from 0% to 300% applied strain. The primary cause for the slightly reduced capacitance may be the degradation of contacts between the gel electrolyte and the electrode in the initial relaxation process, which leads to an increased resistance of the whole device (Figure 5d). The electrochemical stability of the supercapacitor is of paramount importance for the durability of the device in long-term use. Experimental testing shows that after 10000 GCD cycles at a scan rate of 1 A/g, the normalized capacitance reduces by ∼15% (Figure 5i). Most of the reduction in electrochemical performance occurs during the first 2000 cycles, and the capacitance remains nearly constant after 4000 cycles. This phenomenon indicates the contact between materials remains intact and there is minimal film delamination or damage occurring during the stability test, which is promising for realization of this composite system in practical applications.

The volumetric and gravimetric capacitances of stretchable MXene/RGO composite electrodes and supercapacitors are also calculated and compared in Figure S9. The thickness of the film electrode is ∼1 μm, which is estimated by AFM scans of the step height of MXene/RGO composite films on a silicon substrate (Figure S11). The calculated volumetric and gravimetric capacitance for the MXene/RGO composite electrodes is around 350−490 F/cm^3 and 110−160 F/g at a scan rate of 0.5 A/g. High volumetric capacitance of stretchable MXene/RGO composite can be partially attributed to the high volumetric capacitance of MXene components. Figure S10 presents the electrochemical performance of a pure RGO thin film electrode. The distorted CV shape at 50 mV/s and the low slope in the low frequency region of the Nyquist plot indicate the low conductivity of the RGO thin film. Volumetric capacitance of RGO electrode at the scan rate of 1 A/g is 216 F/cm^3, significantly smaller than the value of MXene/RGO composite electrodes due to the smaller

https://dx.doi.org/10.1021/acsnano.9b10066
ACS Nano 2020, 14, 3576−3586

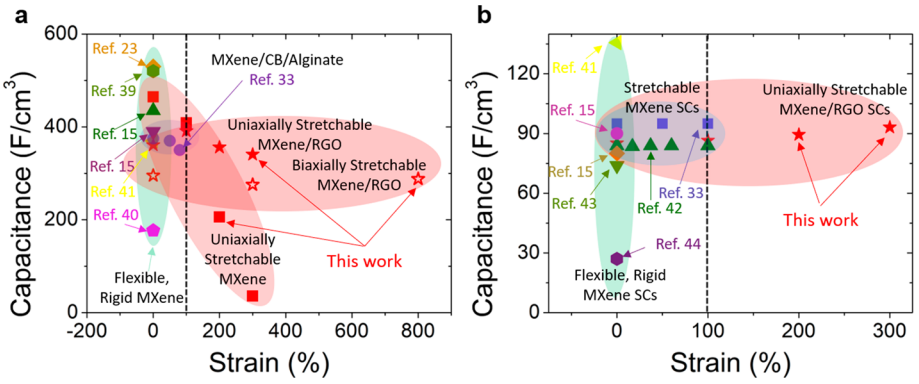

Figure 6. Performance comparison of the developed stretchable $Ti_3C_2T_x$ MXene/RGO composite electrodes and supercapacitors with other $Ti_3C_2T_x$ MXene based electrodes and supercapacitors reported in literature. (a) Comparison of the different electrode performances. The capacitances of $Ti_3C_2T_x$ MXene/RGO electrodes were obtained from GCD measurements at 1 A/g. Key: red stars, uniaxially stretchable $Ti_3C_2T_x$ MXene/RGO composite electrode; hollow stars, biaxially stretchable $Ti_3C_2T_x$ MXene/RGO composite electrode; squares, stretchable pure $Ti_3C_2T_x$ MXene electrode; diamonds, $Ti_3C_2T_x$/PVA film;[23] hexagons, d-$Ti_3C_2T_x$ under 10 MPa;[39] up triangles, sandwiched $Ti_3C_2T_x$/RGO;[15] down triangles, $Ti_3C_2T_x$/single wall carbon nanotube;[15] circles, $Ti_3C_2T_x$/carbon black/sodium alginate;[32] pentagon, $Ti_3C_2T_x$,[40] left triangles, flexible $Ti_3C_2T_x$/RGO.[41] (b) Comparison of the supercapacitor performance. The capacitances of $Ti_3C_2T_x$ MXene/RGO supercapacitor were obtained from GCD measurements at 0.1 A/g. Key: red stars, uniaxially stretchable $Ti_3C_2T_x$ MXene/RGO supercapacitor; squares, $Ti_3C_2T_x$ /carbon black/sodium alginate asymmetric;[32] circles, $Ti_3C_2T_x$ paper;[15] up triangles, kirigami $Ti_3C_2T_x$/bacterial cellulose;[42] diamonds, $Ti_3C_2T_x$/multiwall carbon nanotubes;[15] down triangles, $Ti_3C_2T_x$ paper asymmetric;[43] hexagons, $Ti_3C_2T_x$ seawater electrolyte;[44] left triangles, flexible $Ti_3C_2T_x$/RGO.[41]

volumetric capacitance of RGO. Therefore, the MXene/RGO composite combines the mechanical stability of RGO and large volumetric capacitance of MXene to realize a stretchable electrode with high electrochemical performance.

Figure 6a presents a comparison of the electrochemical performance of the MXene/RGO composite electrodes with other MXene based electrodes reported in literature, in which the specific volumetric capacitances of various MXene electrodes are plotted versus applied strains. It is obvious that our stretchable MXene/RGO composite electrodes provide satisfactory specific capacitance and the highest stretchability, up to 800%, achieved among MXene-based electrodes. Moreover, the specific capacitance of the MXene/RGO composite electrode remains nearly unchanged at different mechanical strains, whereas the pure MXene electrode fabricated by the same process demonstrates a significant loss of capacitance, from 464 F/cm^3 under 0% strain to 36 F/cm^3 under 300% strain. Figure 6b shows the electrochemical performance of the stretchable MXene/RGO composite supercapacitors together with MXene-based supercapacitors. The stretchable MXene/RGO supercapacitors demonstrate a similar specific capacitance but a much larger stretchability compared with other MXene devices, either stretchable or rigid. Detailed comparisons of stretchable MXene/RGO electrodes and supercapacitors with other MXene based devices are listed in Tables S1 and S2. While a narrow voltage window was used in this proof of concept study, the electrodes produced by the same fabrication process should allow operation in a 1 V window in acidic electrolyte[21] or even a wider window in neutral aqueous[45] or organic electrolytes,[46] showing even higher capacitance values and a much larger energy density.

CONCLUSIONS

A simple process for fabricating highly stretchable MXene/RGO composite thin film electrodes and supercapacitors is presented. The MXene/RGO composite film electrodes maintain their electrical conductivity and structural integrity during the fabrication process and operation because of the small mechanical modulus of the hybrid film, strong intersheet interactions, and large nanoflake size of RGO. The measurements show that the MXene/RGO supercapacitor electrodes have suitable performance, which is indicated by a capacitance of 49 mF/cm^2 (~490 F/cm^3 and ~140 F/g) coupled with mechanical stretchability (*i.e.*, up to 300% uniaxial and 200% × 200% biaxial strain) and stable electrochemical properties during mechanical cycling. It was also demonstrated that an all-solid-state supercapacitor with PVA-H_2SO_4 gel electrolyte can achieve a specific capacitance of 18.6 mF/cm^2 (~90 F/cm^3 and ~29 F/g) and electrochemical stability under various strain conditions over 10000 electrochemical cycles. Owing to the superior electrochemical and mechanical performance of the composite electrode, the stretchable MXene/RGO supercapacitor is expected to have broad applications in wearable and stretchable electronics.

MATERIALS AND METHODS

$Ti_3C_2T_x$ MXene Synthesis. $Ti_3C_2T_x$ (MXene) was synthesized by the selective etching of Al from Ti_3AlC_2. Commercial Ti_2AlC powder (Kanthal, Sweden) was mixed with TiC in a 1:1 molar ratio and ball milled for 18 h. Then the mixture was heated to 1350 °C with a ramp rate of 5 °C/min in a tube furnace under flowing Ar gas. The obtained brick was ground with a TiN coated milling bit and sieved through a 400 mesh for powder of <38 μm. The Ti_3AlC_2 powder (2 g) was slowly added to a mixture of LiF (3.2 g, 0.08 mM) and 9 M HCl (40 mL) for 5 min to avoid overheating due to the exothermic nature of the reaction. Then the mixture was stirred at 400 rpm for 24 h at 35 °C. After the required reaction time, the mixture was washed through repeated centrifugation at 3500 rpm (2440 rcf) for 3 min until a dilute green supernatant and swollen sediment was found (pH = 5). Then the sediment was redispersed in 100 mL of deionized water and bath sonicated (40 kHz, Branson Ultrasonic Cleaner) for 1 h. To sediment large multilayer particles or nonreacted MAX phase, the solution was centrifuged at 3500 rpm (2440 rcf) for 1 h, and the supernatant was collected for fabrication of stretchable composites. The concentration of $Ti_3C_2T_x$ solution was ~5 mg/mL.

Reduced Graphene Oxide Synthesis. Reduced graphene oxide (RGO) was synthesized by hydrazine reduction.[47] In brief, 8 mL of

https://dx.doi.org/10.1021/acsnano.9b10066
ACS Nano 2020, 14, 3576−3586

graphene oxide solution (5 mg/mL, Graphene Supermarket, USA) was diluted in 72 mL deionized water (Synergy UV, Millipore, Inc.) in a glass bottle. The graphene oxide solution was then mixed with 0.28 mL 28% ammonia–water and 80 μL 35% hydrazine. After stirring for 3 min, the solution was cured in a water bath (~85 °C) for 1 h with vigorous stirring to reduce the GO for further experimental use.

Fabrication of MXene/RGO Composite Film. The as-prepared MXene solution and RGO solution were mixed in deionized water (Synergy UV, Millipore, Inc.) and sonicated for 20 min to obtain a uniformly dispersed MXene/RGO solution with an RGO weight percentage of 0%, 25%, 50%, 75%, and 100%. The MXene/RGO films were then fabricated by a vacuum-assisted filtration method. The MXene/RGO solution was filtered by a nitrocellulose membrane (0.05 μm pore size, Merck Millipore LTD, Ireland). The resulting MXene/RGO film on the filter membrane was rinsed with DI water to remove the excess hydrazine and ammonia and then immediately immersed in a H_2SO_4 solution (1 M) and stored in a nitrogen box for 24 h. The MXene/RGO film was then rinsed with the DI water and used for the stretchable electrode fabrication.

Lateral Force Microscopy Measurement. LFM measurements were conducted with an Asylum AFM MPF3D in ambient environment, using antimony *n*-doped Si cantilevers (BRUKER Model TRESPA-300, spring constant 40 N/m). Topographic height profiles were obtained by tapping mode imaging using a scan size of 20 μm × 20 μm, a scan rate of 0.5 Hz, and a scan angle of 90 deg. Lateral force images were obtained in contact mode with a tip set point of 800 mV (4.12 μN), scan size 20 μm × 20 μm, and a scan rate of 0.3 Hz. The lateral force was calculated by subtracting the lateral signal from the retrace to trace in the friction loops.

Electrochemical Measurements. The stretchable MXene/RGO electrodes were tested with a three-electrode setup utilizing a Bio-Logic SP-200 potentiostat. All the measurements for the stretchable electrodes were performed with the 1 M H_2SO_4 electrolyte solution. Gel electrolyte of PVA-H_2SO_4 was used for solid-state supercapacitor measurements. Ag/AgCl in saturated KCl was used as the reference electrode and a Pt mesh was used as the counter electrode. Pt wire was utilized as the current collector for the working electrodes, limiting the voltage window. CV curves were measured conservatively in the voltage window from −0.2 to 0.2 V *vs* Ag/AgCl, where double-layer storage dominates, for all the samples as the goal of the work was to demonstrate stretchable devices rather that achieve the maximum possible energy density values. Larger cathodic potential was not applied due to the high hydrogen catalytical activity of the Pt wire. The scan rate was set to range from 5 mV/s to 200 mV/s. Constant current charge/discharge tests were performed in the range from −0.2 to +0.2 V with current densities varying from 0.5 to 10 A/g. EIS measurements of MXene/RGO composite electrode were performed at open-circuit-potential (OCP) with the frequency from 200 kHz to 100 mHz, and the amplitude of 10 mV. EIS of the MXene film electrode was measured at 0 V at the same frequency and sinusoidal amplitude. For the MXene/RGO supercapacitor, the CV measurements were performed from 0 to 0.4 V with a scan rate varying from 5 to 200 mV/s. Galvanostatic charge/discharge (GCD) tests were performed from 0.1 to 2 A/g. EIS was performed at 0 V with frequency from 200 kHz to 100 mHz and amplitude of 10 mV. Electrochemical stability was tested at a constant current charge/discharge rate of 1 A/g when the supercapacitor was relaxed at 0% strain. Due to the low accuracy of measurements when material volumes and/or masses are very small, the areal capacitance is mainly presented for stretchable MXene/RGO composite electrodes and supercapacitors based on the electrode area before prestrain relaxation. Volumetric and gravimetric capacitances are also calculated and presented to exhibit the electrochemical performance of the devices. Volumetric capacitances and stretchability of the electrodes and supercapacitors are compared because this metric is widely adapted in previous literature where areal capacitance are not always provided.

Fabrication of All Solid-State Stretchable Supercapacitors. Two stretchable electrodes were first prepared by dry-transferring MXene/RGO film onto prestrained elastomer substrates (VHB 4910, 3 M Inc., US) following the steps shown in the main text. Then the electrolyte was made by adding 2.5 g of poly(vinyl) alcohol (PVA, MW 146000–186000, Sigma-Aldrich, Inc.) to 25 mL of 1 M H_2SO_4. The solution was further heated up to 90 °C in an oil bath for 1 h with stirring until it became clear. After cooling, the as-prepared PVA-H_2SO_4 gel was cast onto the top surfaces of stretched MXene/RGO electrodes, leaving a small margin area uncovered for connecting the Pt wire current collectors for electrochemical measurements. After drying in air for about 1 h, the two prestretched MXene/RGO electrodes were assembled together to form a double layer electrochemical supercapacitor. In this device, the PVA-H_2SO_4 gel serves as both electrolyte and separator. The assembled device was then tested by a standard two-electrode setup.

MXene and RGO Characterization. Scanning electron microscope (SEM) images were taken using a FEI XL30 system and a FEI Apreo S system. Atomic Force microscopy (AFM) images were taken by using an Asylum AFM MPF3D system and a Digital Instruments Dimension 3100 system. Raman analyses were carried out at room temperature with a 633 nm later excitation, using a Horiba Jobin Yvon LabRAM ARAMIS system. X-ray photoelectron spectroscopy was performed by using a Kratos Analytical Axis Ultra system. Resistance of the thin films was measured in the diagonal direction by using a Flukes 77 IV Multimeter. The average of five measurements is reported.

ASSOCIATED CONTENT

Supporting Information

The Supporting Information is available free of charge at https://pubs.acs.org/doi/10.1021/acsnano.9b10066.

Morphology of the biaxially stretching SC electrodes from MXene/RGO thin films; variation of the electrical resistance of MXene/RGO thin films; characterization of the RGO flakes; strain stress curves of MXene/RGO composite film with different MXene percentages; AFM, CV and EIS measurements of the stretchable electrodes made of MXene and MXene/RGO composite; volumetric capacitances of the MXene/RGO composite electrodes and supercapacitors; Raman and XPS spectra of the MXene and RGO films; comparison of stretchable MXene/RGO electrodes with other MXene based electrodes and supercapacitors reported in the literature (PDF)

AUTHOR INFORMATION

Corresponding Authors

Jeffrey T. Glass − *Department of Mechanical Engineering & Materials Science and Department of Electrical & Computer Engineering, Duke University, Durham, North Carolina 27708, United States*; Email: jeff.glass@duke.edu

Changyong Cao − *Laboratory for Soft Machines & Electronics, School of Packaging, Michigan State University, East Lansing, Michigan 48824, United States; Departments of Mechanical Engineering, Electrical and Computer Engineering, Michigan State University, East Lansing, Michigan 48824, United States;* orcid.org/0000-0001-5067-1716; Email: ccao@msu.edu

Authors

Yihao Zhou − *Department of Mechanical Engineering & Materials Science, Duke University, Durham, North Carolina 27708, United States*

Kathleen Maleski − *A. J. Drexel Nanomaterials Institute, and Department of Materials Science and Engineering, Drexel University, Philadelphia, Pennsylvania 19104, United States;* orcid.org/0000-0003-4032-7385

https://dx.doi.org/10.1021/acsnano.9b10066
ACS Nano 2020, 14, 3576–3586

Babak Anasori − *A. J. Drexel Nanomaterials Institute, and Department of Materials Science and Engineering, Drexel University, Philadelphia, Pennsylvania 19104, United States;* orcid.org/0000-0002-1955-253X

James O. Thostenson − *Department of Electrical & Computer Engineering, Duke University, Durham, North Carolina 27708, United States;* orcid.org/0000-0002-5494-482X

Yaokun Pang − *Laboratory for Soft Machines & Electronics, School of Packaging, Michigan State University, East Lansing, Michigan 48824, United States*

Yaying Feng − *Department of Mechanical Engineering & Materials Science, Duke University, Durham, North Carolina 27708, United States*

Kexin Zeng − *Laboratory for Soft Machines & Electronics, School of Packaging, Michigan State University, East Lansing, Michigan 48824, United States*

Charles B. Parker − *Department of Electrical & Computer Engineering, Duke University, Durham, North Carolina 27708, United States*

Stefan Zauscher − *Department of Mechanical Engineering & Materials Science, Duke University, Durham, North Carolina 27708, United States;* orcid.org/0000-0002-2290-7178

Yury Gogotsi − *A. J. Drexel Nanomaterials Institute, and Department of Materials Science and Engineering, Drexel University, Philadelphia, Pennsylvania 19104, United States;* orcid.org/0000-0001-9423-4032

Complete contact information is available at: https://pubs.acs.org/10.1021/acsnano.9b10066

Notes

The authors declare no competing financial interest.

ACKNOWLEDGMENTS

Y.Z., C.B.P., and J.T.G acknowledge financial support from the National Science Foundation (NSF) (ECCS-1344745). Y.P. and C.C. acknowledge financial support from the start-up fund at Michigan State University and financial support from the USDA National Institute of Food and Agriculture (Hatch Project 1016788). This work was performed in part at the Shared Materials Instrumentation Facility (SMIF) of Duke University, a member of the North Carolina Research Triangle Nanotechnology Network (RTNN), which is supported by the NSF (ECCS-1542015) as part of the National Nanotechnology Coordinated Infrastructure (NNCI). MXene research at Drexel University was sponsored by the Fluid Interface Reactions, Structures, and Transport (FIRST) Center, an Energy Frontier Research Center (EFRC) funded by the U.S. Department of Energy, Office of Science, and Office of Basic Energy Sciences.

REFERENCES

(1) Park, S.-I.; Xiong, Y.; Kim, R.-H.; Elvikis, P.; Meitl, M.; Kim, D.-H.; Wu, J.; Yoon, J.; Yu, C.-J.; Liu, Z.; Huang, Y.; Hwang, K.-c.; Ferreira, P.; Li, X.; Choquette, K.; Rogers, J. A. Printed Assemblies of Inorganic Light-Emitting Diodes for Deformable and Semitransparent Displays. *Science* **2009**, *325*, 977−981.

(2) Li, S.; Peele, B. N.; Larson, C. M.; Zhao, H.; Shepherd, R. F. A Stretchable Multicolor Display and Touch Interface Using Photopatterning and Transfer Printing. *Adv. Mater.* **2016**, *28*, 9770−9775.

(3) Lipomi, D. J.; Vosgueritchian, M.; Tee, B. C. K.; Hellstrom, S. L.; Lee, J. A.; Fox, C. H.; Bao, Z. Skin-Like Pressure and Strain Sensors Based on Transparent Elastic Films of Carbon Nanotubes. *Nat. Nanotechnol.* **2011**, *6*, 788−792.

(4) Sokolov, A. N.; Tee, B. C. K.; Bettinger, C. J.; Tok, J. B. H.; Bao, Z. Chemical and Engineering Approaches To Enable Organic Field-Effect Transistors for Electronic Skin Applications. *Acc. Chem. Res.* **2012**, *45*, 361−371.

(5) Yan, C.; Deng, W.; Jin, L.; Yang, T.; Wang, Z.; Chu, X.; Su, H.; Chen, J.; Yang, W. Epidermis-Inspired Ultrathin 3D Cellular Sensor Array for Self-Powered Biomedical Monitoring. *ACS Appl. Mater. Interfaces* **2018**, *10*, 41070−41075.

(6) Gao, W.; Emaminejad, S.; Nyein, H. Y. Y.; Challa, S.; Chen, K.; Peck, A.; Fahad, H. M.; Ota, H.; Shiraki, H.; Kiriya, D.; Lien, D.-H.; Brooks, G. A.; Davis, R. W.; Javey, A. Fully Integrated Wearable Sensor Arrays for Multiplexed *In Situ* Perspiration Analysis. *Nature* **2016**, *529*, 509−514.

(7) Lu, Y.; Biswas, M. C.; Guo, Z.; Jeon, J.-W.; Wujcik, E. K. Recent Developments in Bio-monitoring *via* Advanced Polymer Nanocomposite-Based Wearable Strain Sensors. *Biosens. Bioelectron.* **2019**, *123*, 167−177.

(8) Zheng, Q.; Shi, B.; Fan, F.; Wang, X.; Yan, L.; Yuan, W.; Wang, S.; Liu, H.; Li, Z.; Wang, Z. L. *In Vivo* Powering of Pacemaker by Breathing-Driven Implanted Triboelectric Nanogenerator. *Adv. Mater.* **2014**, *26*, 5851−5856.

(9) Chatterjee, S.; Saxena, M.; Padmanabhan, D.; Jayachandra, M.; Pandya, H. J. Futuristic Medical Implants Using Bioresorbable Materials and Devices. *Biosens. Bioelectron.* **2019**, *142*, 111489.

(10) Song, W.-J.; Yoo, S.; Song, G.; Lee, S.; Kong, M.; Rim, J.; Jeong, U.; Park, S. Recent Progress in Stretchable Batteries for Wearable Electronics. *Batteries Supercaps* **2019**, *2*, 181−199.

(11) An, T.; Cheng, W. Recent Progress in Stretchable Supercapacitors. *J. Mater. Chem. A* **2018**, *6*, 15478−15494.

(12) Cao, C.; Chu, Y.; Zhou, Y.; Zhang, C.; Qu, S. Recent Advances in Stretchable Supercapacitors Enabled by Low-Dimensional Nanomaterials. *Small* **2018**, *14*, 1803976.

(13) Anasori, B.; Xie, Y.; Beidaghi, M.; Lu, J.; Hosler, B. C.; Hultman, L.; Kent, P. R. C.; Gogotsi, Y.; Barsoum, M. W. Two-Dimensional, Ordered, Double Transition Metals Carbides (MXenes). *ACS Nano* **2015**, *9*, 9507−9516.

(14) Naguib, M.; Mashtalir, O.; Carle, J.; Presser, V.; Lu, J.; Hultman, L.; Gogotsi, Y.; Barsoum, M. W. Two-Dimensional Transition Metal Carbides. *ACS Nano* **2012**, *6*, 1322−1331.

(15) Zhao, M.-Q.; Ren, C. E.; Ling, Z.; Lukatskaya, M. R.; Zhang, C.; Van Aken, K. L.; Barsoum, M. W.; Gogotsi, Y. Flexible MXene/Carbon Nanotube Composite Paper with High Volumetric Capacitance. *Adv. Mater.* **2015**, *27*, 339−345.

(16) Tang, Q.; Zhou, Z.; Shen, P. Are MXenes Promising Anode Materials for Li Ion Batteries? Computational Studies on Electronic Properties and Li Storage Capability of Ti_3C_2 and $Ti_3C_2X_2$ (X = F, OH) Monolayer. *J. Am. Chem. Soc.* **2012**, *134*, 16909−16916.

(17) Cai, Y.; Shen, J.; Ge, G.; Zhang, Y.; Jin, W.; Huang, W.; Shao, J.; Yang, J.; Dong, X. Stretchable $Ti_3C_2T_x$ MXene/Carbon Nanotube Composite Based Strain Sensor with Ultrahigh Sensitivity and Tunable Sensing Range. *ACS Nano* **2018**, *12*, 56−62.

(18) Shahzad, F.; Alhabeb, M.; Hatter, C. B.; Anasori, B.; Man Hong, S.; Koo, C. M.; Gogotsi, Y. Electromagnetic Interference Shielding with 2D Transition Metal Carbides (MXenes). *Science* **2016**, *353*, 1137−1140.

(19) Anasori, B.; Gogotsi, Y. *2D Metal Carbides And Nitrides (MXenes): Structure, Properties and Applications*; Springer: New York, 2019.

(20) Maleski, K.; Mochalin, V. N.; Gogotsi, Y. Dispersions of Two-Dimensional Titanium Carbide MXene in Organic Solvents. *Chem. Mater.* **2017**, *29*, 1632−1640.

(21) Lukatskaya, M. R.; Kota, S.; Lin, Z.; Zhao, M.-Q.; Shpigel, N.; Levi, M. D.; Halim, J.; Taberna, P.-L.; Barsoum, M. W.; Simon, P.; Gogotsi, Y. Ultra-High-Rate Pseudocapacitive Energy Storage in Two-Dimensional Transition Metal Carbides. *Nat. Energy* **2017**, *2*, 17105.

(22) Yan, J.; Ren, C. E.; Maleski, K.; Hatter, C. B.; Anasori, B.; Urbankowski, P.; Sarycheva, A.; Gogotsi, Y. Flexible MXene/Graphene Films for Ultrafast Supercapacitors with Outstanding Volumetric Capacitance. *Adv. Funct. Mater.* **2017**, *27*, 1701264.

(23) Ling, Z.; Ren, C. E.; Zhao, M.-Q.; Yang, J.; Giammarco, J. M.; Qiu, J.; Barsoum, M. W.; Gogotsi, Y. Flexible and Conductive MXene Films and Nanocomposites with High Capacitance. *Proc. Natl. Acad. Sci. U. S. A.* **2014**, *111*, 16676−16681.
(24) Peng, Y.-Y.; Akuzum, B.; Kurra, N.; Zhao, M.-Q.; Alhabeb, M.; Anasori, B.; Kumbur, E. C.; Alshareef, H. N.; Ger, M.-D.; Gogotsi, Y. All-MXene (2D Titanium Carbide) Solid-State Microsupercapacitors for On-Chip Energy Storage. *Energy Environ. Sci.* **2016**, *9*, 2847−2854.
(25) Kurra, N.; Ahmed, B.; Gogotsi, Y.; Alshareef, H. N. MXene-On-Paper Coplanar Microsupercapacitors. *Adv. Energy Mater.* **2016**, *6*, 1601372.
(26) Naguib, M.; Come, J.; Dyatkin, B.; Presser, V.; Taberna, P.-L.; Simon, P.; Barsoum, M. W.; Gogotsi, Y. MXene: APromising Transition Metal Carbide Anode for Lithium-Ion Batteries. *Electrochem. Commun.* **2012**, *16*, 61−64.
(27) Er, D.; Li, J.; Naguib, M.; Gogotsi, Y.; Shenoy, V. B. Ti_3C_2 MXene as a High Capacity Electrode Material for Metal (Li, Na, K, Ca) Ion Batteries. *ACS Appl. Mater. Interfaces* **2014**, *6*, 11173−11179.
(28) Xie, Y.; Dall'Agnese, Y.; Naguib, M.; Gogotsi, Y.; Barsoum, M. W.; Zhuang, H. L.; Kent, P. R. C. Prediction and Characterization of MXene Nanosheet Anodes for Non-Lithium-Ion Batteries. *ACS Nano* **2014**, *8*, 9606−9615.
(29) Come, J.; Xie, Y.; Naguib, M.; Jesse, S.; Kalinin, S. V.; Gogotsi, Y.; Kent, P. R. C.; Balke, N. Nanoscale Elastic Changes in 2D $Ti_3C_2T_x$ (MXene) Pseudocapacitive Electrodes. *Adv. Energy Mater.* **2016**, *6*, 1502290.
(30) Lipatov, A.; Lu, H.; Alhabeb, M.; Anasori, B.; Gruverman, A.; Gogotsi, Y.; Sinitskii, A. Elastic Properties of 2D $Ti_3C_2T_x$ MXene Monolayers and Bilayers. *Sci. Adv.* **2018**, *4*, No. eaat0491.
(31) An, H.; Habib, T.; Shah, S.; Gao, H.; Radovic, M.; Green, M. J.; Lutkenhaus, J. L. Surface-Agnostic Highly Stretchable and Bendable Conductive MXene Multilayers. *Sci. Adv.* **2018**, *4*, No. eaaq0118.
(32) Chang, T.-H.; Zhang, T.; Yang, H.; Li, K.; Tian, Y.; Lee, J. Y.; Chen, P.-Y. Controlled Crumpling of Two-Dimensional Titanium Carbide (MXene) for Highly Stretchable, Bendable, Efficient Supercapacitors. *ACS Nano* **2018**, *12*, 8048−8059.
(33) Liu, J.; Zhang, H.-B.; Xie, X.; Yang, R.; Liu, Z.; Liu, Y.; Yu, Z.-Z. Multifunctional, Superelastic, and Lightweight MXene/Polyimide Aerogels. *Small* **2018**, *14*, 1802479.
(34) Liu, P.; Yang, H.; Zhang, X.; Jiang, M.; Duan, Y.; Zhang, J. Controllable Lateral Contraction and Mechanical Performance of Chemically Reduced Graphene Oxide Paper. *Carbon* **2016**, *107*, 46−55.
(35) Cao, C.; Feng, Y.; Zang, J.; López, G. P.; Zhao, X. Tunable Lotus-Leaf and Rose-Petal Effects *via* Graphene Paper Origami. *Extreme Mech. Lett.* **2015**, *4*, 18−25.
(36) Lin, X.; Shen, X.; Zheng, Q.; Yousefi, N.; Ye, L.; Mai, Y.-W.; Kim, J.-K. Fabrication of Highly-Aligned, Conductive, and Strong Graphene Papers Using Ultralarge Graphene Oxide Sheets. *ACS Nano* **2012**, *6*, 10708−10719.
(37) Borysiuk, V. N.; Mochalin, V. N.; Gogotsi, Y. Bending Rigidity of Two-Dimensional Titanium Carbide (MXene) Nanoribbons: A Molecular Dynamics Study. *Comput. Mater. Sci.* **2018**, *143*, 418−424.
(38) Kwon, S.; Lee, K. E.; Lee, H.; Koh, S. J.; Ko, J.-H.; Kim, Y.-H.; Kim, S. O.; Park, J. Y. The Effect of Thickness and Chemical Reduction of Graphene Oxide on Nanoscale Friction. *J. Phys. Chem. B* **2018**, *122*, 543−547.
(39) Yang, C.; Tang, Y.; Tian, Y.; Luo, Y.; He, Y.; Yin, X.; Que, W. Achieving of Flexible, Free-Standing, Ultracompact Delaminated Titanium Carbide Films for High Volumetric Performance and Heat-Resistant Symmetric Supercapacitors. *Adv. Funct. Mater.* **2018**, *28*, 1705487.
(40) Wang, J.; Tang, J.; Ding, B.; Malgras, V.; Chang, Z.; Hao, X.; Wang, Y.; Dou, H.; Zhang, X.; Yamauchi, Y. Hierarchical Porous Carbons with Layer-By-Layer Motif Architectures from Confined Soft-Template Self-Assembly in Layered Materials. *Nat. Commun.* **2017**, *8*, 15717.
(41) Xu, S.; Wei, G.; Li, J.; Han, W.; Gogotsi, Y. Flexible MXene−Graphene Electrodes with High Volumetric Capacitance for Integrated Co-Cathode Energy Conversion/Storage Devices. *J. Mater. Chem. A* **2017**, *5*, 17442−17451.
(42) Jiao, S.; Zhou, A.; Wu, M.; Hu, H. Kirigami Patterning of MXene/Bacterial Cellulose Composite Paper for All-Solid-State Stretchable Micro-Supercapacitor Arrays. *Adv. Sci.* **2019**, *6*, 1900529.
(43) Wu, W.; Lin, S.; Chen, T.; Li, L.; Pan, Y.; Zhang, M.; Wu, L.; Gao, H.; Zhang, X. Performance Evaluation of Asymmetric Supercapacitor Based on $Ti_3C_2T_x$-Paper. *J. Alloys Compd.* **2017**, *729*, 1165−1171.
(44) Xia, Q. X.; Shinde, N. M.; Zhang, T.; Yun, J. M.; Zhou, A.; Mane, R. S.; Mathur, S.; Kim, K. H. Seawater Electrolyte-Mediated High Volumetric MXene-Based Electrochemical Symmetric Supercapacitors. *Dalton Trans.* **2018**, *47*, 8676−8682.
(45) Anasori, B.; Lukatskaya, M. R.; Gogotsi, Y. 2D Metal Carbides and Nitrides (MXenes) for Energy Storage. *Nat. Rev. Mater.* **2017**, *2*, 16098.
(46) Wang, X.; Mathis, T. S.; Li, K.; Lin, Z.; Vlcek, L.; Torita, T.; Osti, N. C.; Hatter, C.; Urbankowski, P.; Sarycheva, A.; Tyagi, M.; Mamontov, E.; Simon, P.; Gogotsi, Y. Influences From Solvents on Charge Storage in Titanium Carbide MXenes. *Nat. Energy* **2019**, *4*, 241−248.
(47) Li, D.; Müller, M. B.; Gilje, S.; Kaner, R. B.; Wallace, G. G. Processable Aqueous Dispersions of Graphene Nanosheets. *Nat. Nanotechnol.* **2008**, *3*, 101−105.

https://dx.doi.org/10.1021/acsnano.9b10066
ACS Nano 2020, 14, 3576−3586